LLNL-PROC-870363

LAWRENCE LIVERMORE NATIONAL LABORATORY

A Hybrid Second Moment Method for Thermal Radiative Transfer

M. M. Pozulp, T. S. Haut, P. S. Brantley, S. S. Olivier, J. L. Vujic

October 9, 2024

International Conference on Mathematics and Computational Methods Applied to Nuclear Science and Engineering (M&C 2025)
Denver, CO, United States
April 27, 2025 through April 30, 2025

A Hybrid Second Moment Method for Thermal Radiative Transfer

M. Pozulp [1,2,*], T. Haut[1], P. Brantley[1], S. Olivier[3], J. Vujic[2]

[1]Lawrence Livermore National Laboratory, Livermore, CA USA;
[2]University of California, Berkeley, CA USA; [3]Los Alamos National Laboratory, Los Alamos, NM USA

[leave space for DOI, which will be inserted by ANS]

ABSTRACT

We present a hybrid method for solving the equations of thermal radiative transfer. Our method combines the Monte Carlo method with a deterministic method to create a hybrid method. In the Monte Carlo portion of our hybrid method, we use the Monte Carlo particle transport method to solve a linear transport equation without scattering events. In the deterministic portion, we use the finite element method to compute the scattering source term in the linear transport equation. We converge the scattering source in an iteration. We call our method "Hybrid Second Moment", and we demonstrate it by solving a gray, steady-state, linear transport equation in two spatial dimensions.

Keywords: Monte Carlo, finite elements, hybrid

1. INTRODUCTION

The equations of thermal radiative transfer (TRT) are a useful model for the balance of energy in matter and radiation, as long as the matter emissivity is approximately Planckian, the matter absorptivity is approximately proportional to the radiation intensity with a proportionality coefficient that depends only on the temperature and density of the matter, and the radiation frequency band is hard enough that electromagnetic wave effects are insignificant, but soft enough that photo-electronic interactions dominate photo-nuclear.

The TRT system of equations is non-linear. Monte Carlo (MC) methods for TRT often use implicit Monte Carlo (IMC) to linearize the system [1]. The solution to the resulting linear transport equation can be computed using MC particle transport, but the random variability of MC creates statistical noise. Deterministic methods do not have noise, but often discretize phase space dimensions which MC treats as continuous. For example, discrete ordinates (S_N) imposes an angular discretization. This introduces a discretization error called "ray effects", which can be severe as the solution is typically not smooth in angle.

Storing the coefficient matrix for the discrete linear system in S_N discretizations is infeasible because it is very large relative to computer memory capacities. Lagging the scattering source term allows for matrix-free inversion using source iteration (SI) [2]. SI converges arbitrarily slowly in the thick diffusion limit (TDL) [3]. IMC runs arbitrarily slowly in the TDL [4]. Diffusion acceleration can improve SI convergence [5] and IMC runtimes [6, 7, 8]. Moment methods, like Variable Eddington Factor (VEF) and Second Moment Method (SMM), improve SI convergence [9, 10]. Hybrid moment methods improve MC runtimes [11, 12, 13].

We introduce a hybrid moment method called "Hybrid Second Moment" (HSM), which improves on our earlier hybrid method [14]. We still use MC to compute the SMM correction tensor, but we no longer differentiate it, because differentiating a noisy quantity amplifies the noise. We avoid noise amplification by

*pozulp1@llnl.gov, pozulp@berkeley.edu

solving the first-order form of the SMM equations, which has only one derivative on the SMM correction tensor instead of two, and we use a recently-published finite element discretization of the SMM equations to offload the derivative [15]. We also introduce a logical separation of the fixed sources from the scattering source, improve iterative convergence by resetting the pseudo-random number generator seed, and demonstrate the efficacy of HSM by solving a more complicated transport problem which has a non-zero inflow function as well as a non-zero SMM boundary correction factor.

2. HYBRID SECOND MOMENT METHOD

The kernel of the IMC linearization of the TRT system is a linear transport equation with an inflow boundary condition,

$$\mathbf{\Omega} \cdot \nabla\psi + \sigma_t\psi = \frac{\sigma_s}{4\pi}\int \psi \, \mathrm{d}\Omega' + q\,, \tag{1a}$$

$$\psi(\mathbf{x}, \mathbf{\Omega}) = \bar{\psi}(\mathbf{x}, \mathbf{\Omega})\,, \quad \mathbf{x} \in \partial\mathcal{D} \text{ and } \mathbf{\Omega}\cdot\mathbf{n} < 0\,. \tag{1b}$$

See Table I for definitions of the symbols in Equations (1a) and (1b), and all subsequent equations. Define the zeroth, first, and second angular moments of the radiation intensity,

$$\phi(\mathbf{x}) = \int_{\mathbb{S}^2} \psi(\mathbf{x}, \mathbf{\Omega}, E, t)\, \mathrm{d}\Omega\,, \qquad \boldsymbol{J}(\mathbf{x}) = \int_{\mathbb{S}^2} \mathbf{\Omega}\,\psi(\mathbf{x}, \mathbf{\Omega}, E, t)\, \mathrm{d}\Omega\,, \qquad \mathbf{P}(\mathbf{x}) = \int_{\mathbb{S}^2} \mathbf{\Omega}\otimes\mathbf{\Omega}\,\psi(\mathbf{x}, \mathbf{\Omega}, E, t)\, \mathrm{d}\Omega\,. \tag{2}$$

Now take the zeroth and first angular moments of Equation (1a) to get,

$$\nabla\cdot\boldsymbol{J} + \sigma_a\phi = Q_0\,, \tag{3a}$$

$$\nabla\cdot\mathbf{P} + \sigma_t\boldsymbol{J} = \boldsymbol{Q}_1\,, \tag{3b}$$

where Q_0 and $\boldsymbol{Q}_1$ are the zeroth and first angular moments of the fixed source q. The system of Equations (3a) and (3b) is unclosed because it has ten unknowns and only four equations: one radiation relativistic mass (energy) conservation equation and three radiation momentum conservation equations. The independent variables ϕ, $\boldsymbol{J}$, and $\mathbf{P}$ consist of 1+3+6=10 unknowns because they are a scalar, vector, and symmetric tensor.

Derive a boundary condition for Equations (3a) and (3b) by defining $J_n^{\pm} = \int_{\mathbf{\Omega}\cdot\mathbf{n}\gtrless 0} \mathbf{\Omega}\cdot\mathbf{n}\,\psi\,\mathrm{d}\Omega$ where $\mathbf{n}$ is the outward unit normal on the boundary of the domain, and performing algebraic manipulation,

$$\boldsymbol{J}\cdot\mathbf{n} = J_n^- + J_n^+ = 2J_n^- + (J_n^+ - J_n^-) = 2J_n^- + \int_{\mathbb{S}^2} |\mathbf{\Omega}\cdot\mathbf{n}|\,\psi\,\mathrm{d}\Omega\,. \tag{4}$$

Define $B(\psi) = \int_{\mathbb{S}^2} |\mathbf{\Omega}\cdot\mathbf{n}|\,\psi\,\mathrm{d}\Omega$ and $J_{\mathrm{in}} = \int_{\mathbf{\Omega}\cdot\mathbf{n}<0} \mathbf{\Omega}\cdot\mathbf{n}\,\bar{\psi}\,\mathrm{d}\Omega$. The unclosed boundary condition is,

$$\boldsymbol{J}\cdot\mathbf{n} = B(\psi) + 2J_{\mathrm{in}}\,. \tag{5}$$

The SMM closure for the moment system of Equations (3a) and (3b) is $\mathbf{P} = \mathbf{T} + \frac{1}{3}\mathbf{I}\varphi$, where $\mathbf{T} = \int \mathbf{\Omega}\otimes\mathbf{\Omega}\,\psi\,\mathrm{d}\Omega - \frac{1}{3}\mathbf{I}\int\psi\,\mathrm{d}\Omega$ is called the correction tensor. The SMM closure for Equation (5) is $B = \beta + \frac{1}{2}\varphi$, where $\beta(\psi) = \int_{\mathbb{S}^2} |\mathbf{\Omega}\cdot\mathbf{n}|\,\psi\,\mathrm{d}\Omega - \frac{1}{2}\int\psi\,\mathrm{d}\Omega$. Substituting the SMM closures results in the SMM system of equations,

$$\nabla\cdot\boldsymbol{J} + \sigma_a\varphi = Q_0\,, \quad \mathbf{x}\in\mathcal{D}\,, \tag{6a}$$

$$\frac{1}{3}\nabla\varphi + \sigma_t\boldsymbol{J} = \boldsymbol{Q}_1 - \nabla\cdot\mathbf{T}\,, \quad \mathbf{x}\in\mathcal{D}\,, \tag{6b}$$

$$\boldsymbol{J}\cdot\mathbf{n} = \frac{1}{2}\varphi + 2J_{\mathrm{in}} + \beta\,, \quad \mathbf{x}\in\partial\mathcal{D}\,, \tag{6c}$$

where we have switched from using ϕ to φ to emphasize that, even though the SMM system of Equations (6a) to (6c) is an equivalent reformulation of Equations (1a) and (1b), φ can differ from the ϕ defined in Equation (2) after discretization, which is the case for our HSM method.

Figure 1 shows the SMM algorithm. Our HSM method uses the Monte Carlo particle method without scattering events to solve Equation (1a) with boundary condition Equation (1b) (left side of Figure 1) and compute the closures $\mathbf{T}$ and β as Monte Carlo estimators. We then solve Equations (6a) to (6c) (right side of Figure 1) using a deterministic method, and use the solution φ to compute the scattering source, which we converge in an iteration.

$$\varphi$$

$$\begin{aligned} \boldsymbol{\Omega}\cdot\nabla\psi + \sigma_t\psi &= \frac{\sigma_s}{4\pi}\varphi + q\,, \\ \psi(\mathbf{x},\boldsymbol{\Omega}) &= \bar{\psi}(\mathbf{x},\boldsymbol{\Omega})\,, \quad \mathbf{x}\in\partial\mathcal{D} \text{ and } \boldsymbol{\Omega}\cdot\mathbf{n}<0\,. \end{aligned} \qquad \begin{aligned} \nabla\cdot\boldsymbol{J} + \sigma_a\varphi &= Q_0\,, \quad \mathbf{x}\in\mathcal{D}\,, \\ \tfrac{1}{3}\nabla\varphi + \sigma_t\boldsymbol{J} &= \boldsymbol{Q}_1 - \nabla\cdot\mathbf{T}\,, \quad \mathbf{x}\in\mathcal{D}\,, \\ \boldsymbol{J}\cdot\mathbf{n} &= \tfrac{1}{2}\varphi + 2J_{\text{in}} + \beta\,, \quad \mathbf{x}\in\partial\mathcal{D}\,. \end{aligned}$$

$$\begin{aligned} \mathbf{T}(\psi) &= \textstyle\int \boldsymbol{\Omega}\otimes\boldsymbol{\Omega}\,\psi\,\mathrm{d}\Omega - \tfrac{1}{3}\mathbf{I}\int\psi\,\mathrm{d}\Omega \\ \beta(\psi) &= \textstyle\int |\boldsymbol{\Omega}\cdot\mathbf{n}|\,\psi\,\mathrm{d}\Omega - \tfrac{1}{2}\int\psi\,\mathrm{d}\Omega \end{aligned}$$

Figure 1. SMM algorithm [15].

2.1. Deterministic Component of HSM

In Table I, we briefly define some symbols that appear below, such as Y_p and RT_p. Detailed definitions are in [15]. The finite element method weak form for the mixed problem is: find $(\varphi, \boldsymbol{J}) \in Y_p \times RT_p$ such that,

$$\int u\,\nabla\cdot\boldsymbol{J}\,\mathrm{d}\mathbf{x} + \int \sigma_a\,u\varphi\,\mathrm{d}\mathbf{x} = \int u\,Q_0\,\mathrm{d}\mathbf{x}\,, \quad \forall u \in Y_p\,, \tag{7a}$$

$$\begin{aligned} -\frac{1}{3}\int \nabla\cdot\boldsymbol{v}\,\varphi\,\mathrm{d}\mathbf{x} + \int \sigma_t\,\boldsymbol{v}\cdot\boldsymbol{J}\,\mathrm{d}\mathbf{x} + \frac{2}{3}\int_{\Gamma_b}(\boldsymbol{v}\cdot\mathbf{n})(\boldsymbol{J}\cdot\mathbf{n})\,\mathrm{d}s &= \int \boldsymbol{v}\cdot\boldsymbol{Q}_1\,\mathrm{d}\mathbf{x} - \int_{\Gamma_b}\boldsymbol{v}\cdot\mathbf{Tn}\,\mathrm{d}s \\ &\quad + \frac{2}{3}\int_{\Gamma_b}(\boldsymbol{v}\cdot\mathbf{n})(2J_{\text{in}}+\beta)\,\mathrm{d}s - \int_{\Gamma_0}[\![v]\!]\cdot\{\!\{\mathbf{Tn}\}\!\}\,\mathrm{d}s + \int \nabla_h\boldsymbol{v} : \mathbf{T}\,\mathrm{d}\mathbf{x} \quad \forall v \in RT_p\,, \end{aligned} \tag{7b}$$

where the "broken" gradient ∇_h, the jump operator $[\![\cdot]\!]$, and the average operator $\{\!\{\cdot\}\!\}$ are defined as,

$$(\nabla_h u)|_K = \nabla(u|_K) \;\; \forall K \in \mathcal{T}\,, \qquad [\![u]\!] = \begin{cases} u_1 - u_2 & \mathcal{F}\in\Gamma_0 \\ u & \mathcal{F}\in\Gamma_b \end{cases}\,, \qquad \{\!\{u\}\!\} = \begin{cases} \dfrac{u_1+u_2}{2} & \mathcal{F}\in\Gamma_0 \\ u & \mathcal{F}\in\Gamma_b \end{cases}\,. \tag{8}$$

To derive Equation (7a), let $u \in Y_p$, multiply Equation (6a) by u, then integrate over $\mathcal{D}$. Deriving Equation (7b) requires several steps and employs integration by parts (IBP) rules created using the following vector calculus identities:

- Product rule for divergence of a scalar (a) times a vector ($\boldsymbol{F}$):

$$\nabla\cdot(a\boldsymbol{F}) = \nabla a\cdot\boldsymbol{F} + a\nabla\cdot\boldsymbol{F}\,, \tag{9}$$

- Divergence theorem:
$$\int_K \nabla \cdot \boldsymbol{F}\,\mathrm{d}\mathbf{x} = \int_{\partial K} \boldsymbol{F} \cdot \mathbf{n}\,\mathrm{d}s\,, \tag{10}$$
- Product rule for divergence of a vector ($\boldsymbol{v}$) dotted with a tensor ($\mathbf{T}$):
$$\nabla \cdot (\boldsymbol{v} \cdot \mathbf{T}) = \boldsymbol{v} \cdot (\nabla \cdot \mathbf{T}) + \mathbf{T} : \nabla \boldsymbol{v}\,, \tag{11}$$
- Double dot product involving vectors ($\boldsymbol{v}$, $\mathbf{n}$) and a tensor ($\mathbf{T}$):
$$(\boldsymbol{v} \cdot \mathbf{T}) \cdot \mathbf{n} = \boldsymbol{v} \cdot (\mathbf{T}\mathbf{n})\,. \tag{12}$$

Combining Equation (9) with Equation (10) gives an IBP rule that offloads a derivative from a scalar trial function to a vector test function and produces a surface integral as a side effect,
$$\int \nabla a \cdot \boldsymbol{F}\,\mathrm{d}\mathbf{x} = -\int a \nabla \cdot \boldsymbol{F}\,\mathrm{d}\mathbf{x} - \int_{\partial K} a(\boldsymbol{F} \cdot \mathbf{n})\,\mathrm{d}s\,. \tag{13}$$

Combining Equation (11) with Equation (10) gives an IBP rule that offloads a derivative from a tensor function to a vector test function and produces a surface integral as a side effect. Subsequent use of Equation (12) in the integrand of the surface integral gives,
$$\int \boldsymbol{v} \cdot \nabla \cdot \mathbf{T}\,\mathrm{d}\mathbf{x} = -\int \mathbf{T} : \nabla \boldsymbol{v}\,\mathrm{d}\mathbf{x} - \int_{\partial K} \boldsymbol{v} \cdot \mathbf{T}\mathbf{n}\,\mathrm{d}s\,. \tag{14}$$

The three steps for deriving Equation (7b) are as follows:

2.1.1. Step 1) Integration over element K

Integrating Equation (6b) over an arbitrary finite element K and applying the IBP rules in Equations (13) and (14) gives,
$$\begin{aligned} -\frac{1}{3}\int_K \nabla \cdot \boldsymbol{v}\,\varphi\,\mathrm{d}\mathbf{x} + \frac{1}{3}\int_{\partial K} \varphi\,(\boldsymbol{v} \cdot \mathbf{n})\,\mathrm{d}s + \int_K \sigma_t\,\boldsymbol{v} \cdot \boldsymbol{J}\,\mathrm{d}\mathbf{x} \\ = \int_K \boldsymbol{v} \cdot \boldsymbol{Q}_1\,\mathrm{d}\mathbf{x} - \int_{\partial K} \boldsymbol{v} \cdot \mathbf{T}\mathbf{n}\,\mathrm{d}s + \int_K \nabla \boldsymbol{v} : \mathbf{T}\,\mathrm{d}\mathbf{x} \quad \forall v \in RT_p\,. \end{aligned} \tag{15}$$

2.1.2. Step 2) Sum over all elements

Summing Equation (15) over all elements $K \in \mathcal{T}$ gives,
$$\begin{aligned} -\frac{1}{3}\int \nabla \cdot \boldsymbol{v}\,\varphi\,\mathrm{d}\mathbf{x} + \frac{1}{3}\int_{\partial \mathcal{D}} \varphi\,(\boldsymbol{v} \cdot \mathbf{n})\,\mathrm{d}s + \int \sigma_t\,\boldsymbol{v} \cdot \boldsymbol{J}\,\mathrm{d}\mathbf{x} \\ = \int \boldsymbol{v} \cdot \boldsymbol{Q}_1\,\mathrm{d}\mathbf{x} - \int_{\partial \mathcal{D}} \boldsymbol{v} \cdot \mathbf{T}\mathbf{n}\,\mathrm{d}s - \int_{\Gamma_0} [\![v]\!] \cdot \{\!\{ \mathbf{T}\mathbf{n} \}\!\}\,\mathrm{d}s + \int \nabla_h \boldsymbol{v} : \mathbf{T}\,\mathrm{d}\mathbf{x} \quad \forall v \in RT_p\,. \end{aligned} \tag{16}$$

2.1.3. Step 3) Enforce boundary condition

Solving Equation (6c) for φ and substituting into the second term in Equation (16) gives the final result, Equation (7b).

2.2. Monte Carlo Component of HSM

Consider the iteration diagram in Figure 1 once more. The MC particle transport method, which we use to compute the solution to the linear transport equation, incorporates the SMM solution φ shown on the top edge of the diagram, which allows us to neglect scattering events while tracking the MC particles. This removes effective scattering events from IMC photon histories, which makes the histories significantly shorter in the optically-thick, highly absorbing matter that characterizes the TDL.

The bottom edge of the iteration diagram shows the SMM data, $\mathbf{T}$ and β, which we compute during the Monte Carlo solve. Let $\hat{\mathbf{T}} = \hat{\mathbf{P}} - \frac{1}{3}\mathbf{I}\hat{\phi}$ and $\hat{\beta} = \hat{B} - \frac{1}{2}\hat{\phi}_s$ be MC estimators for $\mathbf{T}$ and β where,

$$\hat{\phi} = \frac{1}{V}\sum_i d_i w_i\,, \qquad \hat{\mathbf{P}} = \frac{1}{V}\sum_i \mathbf{\Omega}_i \otimes \mathbf{\Omega}_i\, d_i w_i\,, \qquad \hat{B} = \frac{2}{A}\sum_i w_i\,, \qquad \hat{\phi}_s = \frac{2}{A}\sum_i \frac{w_i}{|\mathbf{\Omega}_i \cdot \mathbf{n}|}\,. \tag{17}$$

Both $\hat{\phi}$ and $\hat{\mathbf{P}}$ are path-length estimators, so the sum is over paths of length d_i in the volume V, and path i is traversed by the MC particle with weight w_i moving in the direction $\mathbf{\Omega}_i$. Thus, $\hat{\mathbf{T}}$ is a piecewise-constant tally defined on each element of the mesh. This is in contrast to $\hat{B}$ and $\hat{\phi}_s$ which are sums over MC particles with weight w_i moving in the direction $\mathbf{\Omega}_i$ which pass through a boundary face with area A and unit normal vector $\mathbf{n}$. Thus, β and $\hat{\phi}_s$ are piecewise-constant tallies defined on each boundary face of the mesh.

2.3. Properties of HSM

We hypothesize that the error of the HSM solution is $O(h) + O(N^{-1/2})$. The first term is due to the h^{p+1} convergence of the mixed finite element discretization of the SMM system, where $p = 0$ in our case because we use lowest-order finite elements. Thus, decreasing the numerical error due to the spatial discretization by a factor of 2 requires decreasing the element width h by the same factor. The second term is due to arguments arising from the Central Limit Theorem, and thus decreasing the variance of the MC estimators by a factor of 2 requires increasing the number of MC particles N by a factor of 4.

2.4. Implementation Details of HSM

Algorithm 1 shows how an existing Monte Carlo solver can incorporate HSM. The iteration converges when the relative difference of successive iterates falls below a user-provided threshold η,

$$\max_j(|\hat{\phi}_j^{(i-1)} - \hat{\phi}_j^{(i)}| \;/\; \hat{\phi}_j^{(i-1)}) < \eta\,, \qquad j = 1, \ldots, |\mathcal{T}|\,, \tag{18}$$

where $|\mathcal{T}|$ is the number of elements in the mesh.

2.4.1. Solving the linear system

The mixed FEM SMM system of Equations (7a) and (7b) permits hybridization, which replaces the block system with a smaller system for Lagrange multipliers. The hybridized system has fewer unknowns and is also symmetric positive definite, which means that we can solve it using conjugate gradient (CG) and we can precondition using algebraic multigrid (AMG). AMG coarsening produces small grids with few degrees of freedom, which makes AMG relatively slow on graphics processing units (GPUs), because operations on the coarse grid have an insufficient amount of work to amortize GPU kernel launch overhead. Solvers designed for solving the original system on GPUs may outperform AMG+CG on the hybridized system [16].

Algorithm 1 Hybrid Second Moment

Input: user-provided boolean value *HSM*
if not HSM **then**
  scattering_events $\leftarrow$ true
  $\hat{\phi} \leftarrow$ mc(q, scattering_events)
  return $\hat{\phi}$
end if
scattering_events $\leftarrow$ false
$\hat{\phi}^{(0)}, \hat{\mathbf{T}}^{(0)}, \hat{\beta}^{(0)} \leftarrow$ mc(q, scattering_events)
$i \leftarrow 1$
while not converged($\hat{\phi}^{(i-1)}, \hat{\phi}^{(i)}$) **do**
  $\varphi^{(i)} \leftarrow \mathrm{sm}(Q_0, \boldsymbol{Q}_1, \hat{\mathbf{T}}^{(i-1)}, \hat{\beta}^{(i-1)})$
  $\hat{\phi}_{\text{temp}}, \hat{\mathbf{T}}_{\text{temp}}, \hat{\beta}_{\text{temp}} \leftarrow$ mc($\varphi^{(i)}$, scattering_events)
  $\hat{\phi}^{(i)} \leftarrow \hat{\phi}^{(0)} + \hat{\phi}_{\text{temp}}$
  $\hat{\mathbf{T}}^{(i)} \leftarrow \hat{\mathbf{T}}^{(0)} + \hat{\mathbf{T}}_{\text{temp}}$
  $\hat{\beta}^{(i)} \leftarrow \hat{\beta}^{(0)} + \hat{\beta}_{\text{temp}}$
  $i \leftarrow i + 1$
end while
return $\hat{\phi}^{(i)}$

2.4.2. Sampling fixed sources

The fixed source $q = q(\mathbf{x}, \boldsymbol{\Omega})$ is a volume source. Our method for assigning MC particle weights is,

$$\lim_{N\to\infty} \sum_{i=1}^{N} w_i = \int_{\mathcal{D}} \int_{\mathbb{S}^2} q \, \mathrm{d}\Omega \, \mathrm{d}\mathbf{x} \,, \tag{19a}$$

where N is the number of MC particles sourced in the volume $\mathcal{D}$ and w_i is the weight of particle i. Let $U(a, b)$ be a uniformly-distributed random variate on $[a, b]$. We use Monte Carlo to integrate,

$$\int_{\mathcal{D}} \int_{\mathbb{S}^2} q \, \mathrm{d}\Omega \, \mathrm{d}\mathbf{x} \approx \frac{V}{N} \sum_{i=1}^{N} q(x_i, y_i, z_i, \theta_i, \phi_i) \,, \tag{19b}$$

$$V = \int_{\mathcal{D}} \int_{\mathbb{S}^2} \mathrm{d}\Omega \, \mathrm{d}\mathbf{x} \,, \qquad x_i \leftarrow U(x_{\min}, x_{\max}) \,, \qquad y_i \leftarrow U(y_{\min}, y_{\max}) \,, \tag{19c}$$

$$z_i \leftarrow U(z_{\min}, z_{\max}) \,, \qquad \theta_i \leftarrow \cos^{-1}(U(-1, 1)) \,, \qquad \phi_i \leftarrow U(0, 2\pi) \,, \tag{19d}$$

where we have assumed that $\mathcal{D}$ is a rectangular prism. The fixed source $\bar{\psi}(\mathbf{x}, \boldsymbol{\Omega})$ is a surface source. Our method for assigning MC particle weights is,

$$\lim_{M\to\infty} \sum_{i=1}^{M} w_i = \int_{\partial\mathcal{D}} \int_{\boldsymbol{\Omega}\cdot\mathbf{n}<0} |\boldsymbol{\Omega} \cdot \mathbf{n}| \bar{\psi} \, \mathrm{d}\Omega \, \mathrm{d}\mathbf{x} \,, \tag{20a}$$

where M is the number of MC particles sourced on the surface $\partial\mathcal{D}$ and w_i is the weight of particle i. We use Monte Carlo to integrate,

$$\int_{\partial\mathcal{D}} \int_{\boldsymbol{\Omega}\cdot\mathbf{n}<0} |\boldsymbol{\Omega} \cdot \mathbf{n}| \bar{\psi} \, \mathrm{d}\Omega \, \mathrm{d}\mathbf{x} \approx \frac{S}{M} \sum_{i=1}^{M} |\boldsymbol{\Omega}_i \cdot \mathbf{n}| \bar{\psi}(x_i, y_i, z_i, \theta_i, \phi_i) \,, \tag{20b}$$

$$S = \int_{\partial\mathcal{D}} \int_{\boldsymbol{\Omega}\cdot\mathbf{n}<0} \mathrm{d}\Omega \, \mathrm{d}\mathbf{x} \,, \tag{20c}$$

where $\mathbf{x}_i$ are sampled uniformly in $\partial\mathcal{D}$ and Ω_i are sampled uniformly on the hemisphere of the unit sphere defined by $\boldsymbol{\Omega} \cdot \mathbf{n} < 0$.

2.4.3. Sampling the scattering source

The algorithm for sampling the scattering source resembles that of the fixed source q except in Equations (19a) and (19b) we replace q with the product of $\sigma_s/(4\pi)$ and $\varphi^{(i)}$. We reset the pseudo-random number generator seed every cycle of the HSM iteration, which means that MC particles are sourced with the same position and direction every cycle, but with different weights, because $\varphi^{(i)} \neq \varphi^{(i-1)}$ and so the scattering source that we evaluate to determine the MC particle weights changes every cycle. Figure 2 shows that the HSM iteration converges when we reset the seed ("Seed reset") and that the iteration does not converge if we do not reset the seed ("No seed reset").

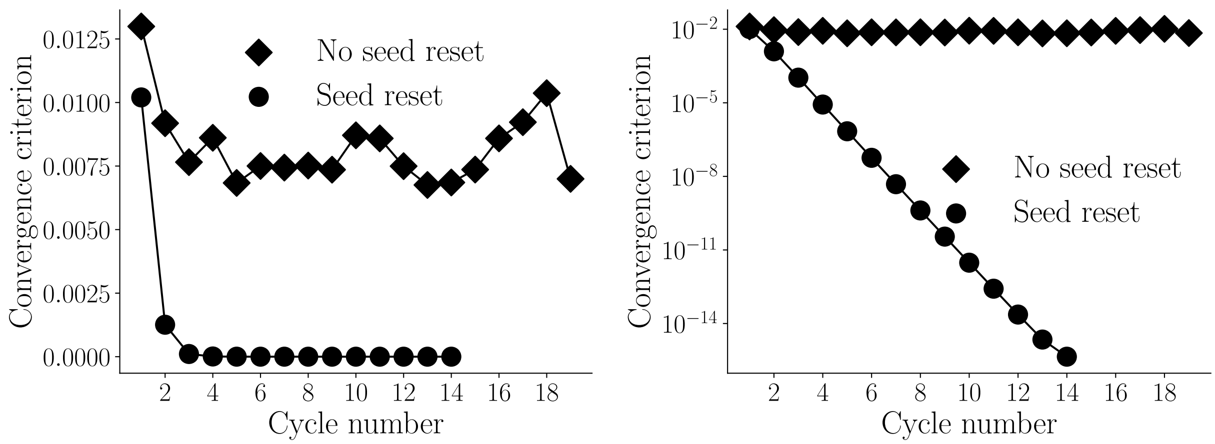

(a) Linear vertical axis. **(b) Logarithmic vertical axis.**

Figure 2. Resetting the pseudo-random number generator seed makes the HSM iteration converge.

3. NUMERICAL RESULTS

We verify the hypothesized convergence rate $O(h)+O(N^{-1/2})$, which defines an error surface that decreases in height as one traverses simultaneously upward and rightward in Figure 3. By making h small and running multiple calculations with increasing N ("particle scaling study"), we observe the $O(N^{-1/2})$ term in the hypothesized convergence rate, and by making N large and running multiple calculations with decreasing h ("element scaling study"), we observe the $O(h)$ term. We use the method of manufactured solutions (MMS). We let $\mathcal{D} = [0, 1]^2$, $\sigma_t = 2$, $\sigma_s = 1$, and we solve the problem specified by Equations (1a) and (1b) for the MMS solution in Equation (89) in [17]. We do this by substituting the MMS solution into Equations (1a) and (1b) and solving for q and $\bar{\psi}$ and using them in the MC component of our HSM solver, and substituting the MMS solution into Equations (6a) to (6c) and solving for Q_0, $\boldsymbol{Q}_1$, and J_{in} and using them in the deterministic component of our HSM solver. The MMS solution, shown in Equation (21), is quadratically-anisotropic so it cannot be computed with the radiation diffusion approximation, it has non-zero closures $\mathbf{T} \neq 0$ and $\beta \neq 0$, and it has non-zero inflow $J_{\text{in}} \neq 0$. The MMS solution is,

$$\psi = \frac{1}{4\pi}\left(\sin(\pi x)\sin(\pi y) + \mathbf{\Omega}_x\mathbf{\Omega}_y \sin(2\pi x)\sin(2\pi y) + \mathbf{\Omega}_x^2 \sin\left(\frac{5\pi}{2}x + \frac{\pi}{4}\right)\sin\left(\frac{5\pi}{2}y + \frac{\pi}{4}\right) + 0.5\right). \tag{21}$$

The results in Figure 4 demonstrate that HSM converges under mesh refinement and MC sample augmentation, and that the rate of convergence with respect to the element width and number of MC particles matches our hypothesis of $O(h) + O(N^{-1/2})$. The slight degradation in convergence at the highest mesh resolution, appearing as liftoff above the dashed curve at the bottom-left of Figure 4b, is expected behavior because we distribute a fixed number of MC particles across more and more elements under mesh refinement. We confirmed that this was the case by running fewer MC particles and observing earlier liftoff.

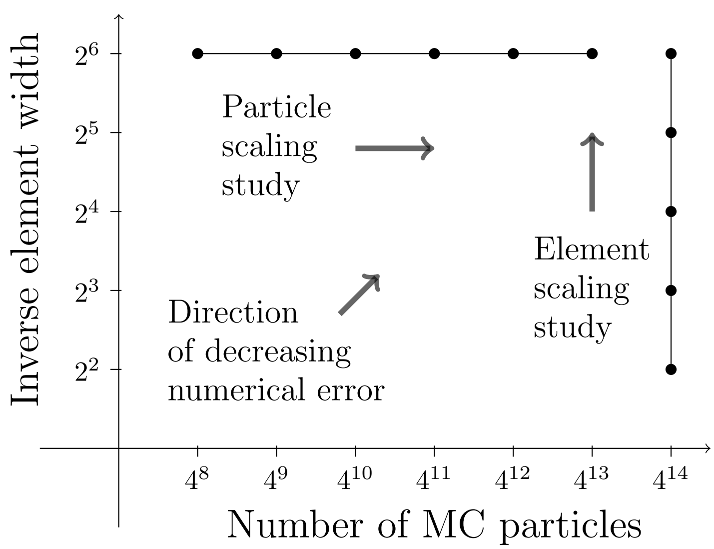

Figure 3. Calculation points on the HSM error surface.

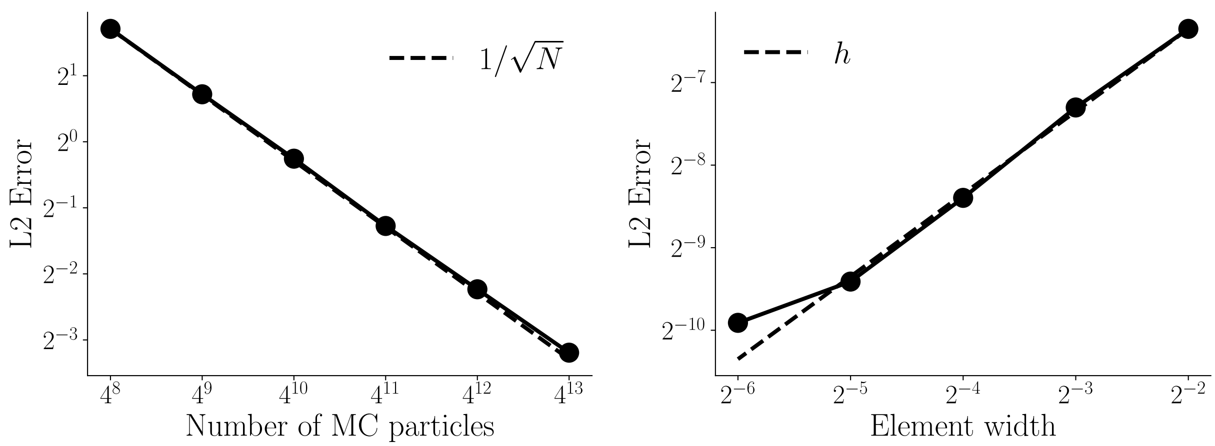

(a) Error as number of MC particles increases. **(b) Error as element width decreases.**

Figure 4. Error of HSM iterate $\phi^{(i)}$ upon convergence.

4. CONCLUSIONS

We presented a hybrid method for solving the equations of thermal radiative transfer. We demonstrated the method by solving a gray, steady-state, linear transport problem in two spatial dimensions. Future work includes running HSM on a multi-material problem with optically-thick and optically-thin regions.

Table I. Nomenclature

Symbol	Name	Symbol	Name
$\mathbf{x}$	position	Y_p	the degree-p Discontinuous Galerkin space
Ω	direction of photon travel	RT_p	the order p Raviart Thomas finite element space
$\psi(\mathbf{x},\Omega)$	radiation intensity	u	finite element test function $u \in Y_p$
$\phi(\mathbf{x})$	0th angular moment of ψ	$\boldsymbol{v}$	finite element test function $\boldsymbol{v} \in RT_p$
ϕ	azimuthal angle of the unit sphere	$\mathcal{F}$	a face in the mesh
θ	polar angle of the unit sphere	Γ	set of unique faces in the mesh
$\boldsymbol{J}(\mathbf{x})$	1st angular moment of ψ	Γ_0	set of unique interior faces in the mesh
$\mathbf{P}(\mathbf{x})$	2nd angular moment of ψ	Γ_b	set of unique faces on the boundary of the mesh
$\sigma_t(\mathbf{x})$	total opacity	K	a finite element
$\sigma_s(\mathbf{x})$	scattering opacity	∂K	the boundary of K
$\sigma_a(\mathbf{x})$	absorption opacity	$\mathcal{T}$	tessellation of the domain $\mathcal{D}$
$q(\mathbf{x},\Omega)$	fixed source	∇	the spatial gradient $\nabla = \frac{\partial}{\partial x}\mathbf{e}_x + \frac{\partial}{\partial y}\mathbf{e}_y + \frac{\partial}{\partial z}\mathbf{e}_z$
$Q_0(\mathbf{x})$	0th angular moment of q	∇_h	the local gradient, $(\nabla_h u)\|_K = \nabla(u\|_K)$, $\forall K \in \mathcal{T}$
$\boldsymbol{Q}_1(\mathbf{x})$	1st angular moment of q	$\nabla\cdot$	the divergence operator
$\mathcal{D}$	computation domain	$\otimes$	the outer product
$\partial\mathcal{D}$	boundary of $\mathcal{D}$	$:$	scalar contraction of two tensors
$\mathbb{S}^2$	the unit sphere	$[\![\cdot]\!]$	the jump of a function across $\mathcal{F}$
$\mathbf{n}$	outward unit normal vector	$\{\!\{\cdot\}\!\}$	average evaluated on both sides of $\mathcal{F}$
$\bar{\psi}(\mathbf{x},\Omega)$	inflow boundary function	h	characteristic mesh element length
φ	solution of the moment system	ϵ	thick diffusion limit parameter
J_{in}	inflow current computed from $\bar{\psi}$	η	iteration convergence tolerance (10^{-3})
$\mathbf{T}$	SMM correction tensor	$U(a,b)$	uniformly randomly distributed variate on $[a,b]$
β	SMM boundary correction factor	$O(\cdot)$	asymptotic order dependence (“Big O” notation)

ACKNOWLEDGEMENTS

The first author greatly appreciates helpful suggestions from the following members of the MC Particle Transport Project at Lawrence Livermore National Laboratory: N. Gentile, M. McKinley, M. O’Brien, A. Robinson, and R. Vega. This work was performed under the auspices of the U.S. Department of Energy by Lawrence Livermore National Laboratory under Contract DE-AC52-07NA27344.

REFERENCES

[1] J. A. Fleck and J. D. Cummings. “An implicit Monte Carlo scheme for calculating time and frequency dependent nonlinear radiation transport.” *J Comput Phys*, **volume 8**, pp. 313–342 (1971).

[2] M. L. Adams and E. W. Larsen. “Fast iterative methods for discrete-ordinates particle transport calculations.” *Progress in Nuclear Energy*, **volume 40**(1), pp. 3–159 (2002).

[3] E. W. Larsen, J. E. Morel, and W. F. Miller Jr. "Asymptotic solutions of numerical transport problems in optically thick, diffusive regimes." *J Comput Phys*, **volume 69**(2), pp. 283–324 (1987). URL https://www.sciencedirect.com/science/article/pii/0021999187901707.

[4] A. B. Wollaber. "Four decades of implicit Monte Carlo." *Journal of Computational and Theoretical Transport* (2016).

[5] R. E. Alcouffe. "Diffusion Synthetic Acceleration Methods for the Diamond-Differenced Discrete-Ordinates Equations." *Nuclear Science and Engineering*, **volume 64**(2), pp. 344–355 (1977). URL https://doi.org/10.13182/NSE77-1.

[6] J. A. Fleck and E. H. Canfield. "A random walk procedure for improving the computational efficiency of the Implicit Monte Carlo method for nonlinear radiation transport." *J Comput Phys*, **volume 54**, pp. 508–523 (1984).

[7] N. Gentile. "Implicit Monte Carlo diffusion - An acceleration method for Monte Carlo time-dependent radiative transfer simulations." *J Comput Phys*, **volume 172**, pp. 543–571 (2001).

[8] J. D. Densmore, T. J. Urbatsch, T. M. Evans, and M. W. Buksas. "A hybrid transport-diffusion method for Monte Carlo radiative-transfer simulations." *Journal of Computational Physics*, **volume 222**(2), pp. 485–503 (2007). URL https://www.sciencedirect.com/science/article/pii/S0021999106003639.

[9] V. Y. Gol'din. "A quasi-diffusion method of solving the kinetic equation." *USSR Computational Mathematics and Mathematical Physics*, **volume 4**, pp. 136–149 (1964).

[10] E. Lewis and W. Miller. "A comparison of p1 synthetic acceleration techniques." *Transactions of the American Nuclear Society*, **volume 23** (1976).

[11] M. A. Cooper and E. W. Larsen. "Automated Weight Windows for Global Monte Carlo Particle Transport Calculations." *Nuclear Science and Engineering*, **volume 137**, pp. 1–13 (2001).

[12] H. Park, D. A. Knoll, R. M. Rauenzahn, A. B. Wollaber, and J. D. Densmore. "A Consistent, Moment-Based, Multiscale Solution Approach for Thermal Radiative Transfer Problems." *Transport Theory and Statistical Physics*, **volume 41**(3-4), pp. 284–303 (2012). URL https://doi.org/10.1080/00411450.2012.671224.

[13] V. N. Novellino and D. Y. Anistratov. "Analysis of Hybrid MC/Deterministic Methods for Transport Problems Based on Low-Order Equations Discretized by Finite Volume Schemes." *Transaction of American Nuclear Society*, **volume 130** (2024).

[14] M. Pozulp, T. Haut, P. Brantley, and J. Vujic. "An Implicit Monte Carlo Acceleration Scheme." In *Proceedings of the International Conference on Mathematics and Computational Methods Applied to Nuclear Science & Engineering (M&C 2023)*. Niagara Falls, Canada (2023).

[15] S. S. Olivier. *High-Order Moment Methods for Thermal Radiative Transfer*. Phd dissertation, University of California, Berkeley, Berkeley, CA (2022).

[16] W. Pazner, T. Kolev, and P. S. Vassilevski. "Matrix-Free High-Performance Saddle-Point Solvers for High-Order Problems in $\boldsymbol{H}(\mathbf{div})$." *SIAM Journal on Scientific Computing*, **volume 46**(3), pp. B179–B204 (2024).

[17] S. Olivier, W. Pazner, T. S. Haut, and B. C. Yee. "A family of independent Variable Eddington Factor methods with efficient preconditioned iterative solvers." *Journal of Computational Physics*, **volume 473**, p. 111747 (2023). URL https://www.sciencedirect.com/science/article/pii/S0021999122008105.